Materials Futures

PAPER • **OPEN ACCESS**

Taking advantage of glass: capturing and retaining the helium gas on the moon

To cite this article: Ao Li *et al* 2022 *Mater. Futures* **1** 035101

OPEN ACCESS
IOP Publishing | Songshan Lake Materials Laboratory
Materials Futures
Mater. Futures 1 (2022) 035101 (7pp)
https://doi.org/10.1088/2752-5724/ac74af

Taking advantage of glass: capturing and retaining the helium gas on the moon

Ao Li[1,2,8], Xiao Chen[1,2,8], Lijian Song[1,2,8], Guoxin Chen[3,8], Wei Xu[1,*], Juntao Huo[1,*], Meng Gao[1], Ming Li[3], Lei Zhang[3], Bingnan Yao[1], Min Ji[1], Yan Zhang[1], Shaofan Zhao[4], Wei Yao[4], Yanhui Liu[5], Jun-Qiang Wang[1,2,*], Haiyang Bai[4,5,*], Zhigang Zou[4,6], Mengfei Yang[4] and Weihua Wang[4,5,7]

[1] CAS Key Laboratory of Magnetic Materials and Devices, and Zhejiang Province Key Laboratory of Magnetic Materials and Application Technology, Ningbo Institute of Materials Technology and Engineering, Chinese Academy of Sciences, Ningbo 315201, People's Republic of China
[2] Center of Materials Science and Optoelectronics Engineering, University of Chinese Academy of Sciences, Beijing 100049, People's Republic of China
[3] Center of Test and Analysis, Ningbo Institute of Materials Technology and Engineering, Chinese Academy of Sciences, Ningbo 315201, People's Republic of China
[4] Qian Xuesen Laboratory of Space Technology, China Academy of Space Technology (CAST), Beijing 100094, People's Republic of China
[5] Institute of Physics, Chinese Academy of Sciences, Beijing 100190, People's Republic of China
[6] College of Engineering and Applied Sciences, Nanjing University, Nanjing 210093, People's Republic of China
[7] Songshan Lake Materials Laboratory, Dongguan, 523830, People's Republic of China

E-mail: weixu@nimte.ac.cn, huojuntao@nimte.ac.cn, jqwang@nimte.ac.cn and hybai@iphy.ac.cn

Received 29 May 2022
Accepted for publication 29 May 2022
Published 24 June 2022

Abstract

Helium-3 (^{3}He) is a noble gas that has critical applications in scientific research and promising application potential as clean fusion energy. It is thought that the lunar regolith contains large amounts of helium, but it is challenging to extract because most helium atoms are reserved in defects of crystals or as solid solutions. Here, we find large amounts of helium bubbles in the glassy surface layer of ilmenite particles that were brought back by the Chang'E-5 mission. The special disordered atomic packing structure of glasses should be the critical factor for capturing the noble helium gas. The reserves in bubbles do not require heating to high temperatures to be extracted. Mechanical methods at ambient temperatures can easily break the bubbles. Our results provide insights into the mechanism of helium gathering on the moon and offer guidance on future *in situ* extraction.

Supplementary material for this article is available online

Keywords: glass, lunar regolith, disorder, helium bubble, ilmenite

[8] These authors contributed equally.
[*] Authors to whom any correspondence should be addressed.

Future perspectives
Lunar regolith contains important resources that are rare on Earth. For example, helium-3, which is much more abundant on the moon than on the earth, is a vital element for nuclear fusion and future developments in energy sectors. Herein, we report abundant helium bubbles in the glassy surface layer of lunar regolith particles. The disordered atomic packing structure of glass plays a critical role in capturing and retaining the noble helium gas. Compared to the helium dissolved in the lunar crystal lattice that requires high temperatures to release, the helium gas contained in bubbles is much easier to extract by using a mechanical milling strategy at ambient temperatures. This demonstrates promising futures for a lunar gold rush.

1. Introduction

The moon has a variety of unique resources, which are important supplements and reserves for the terrestrial resources and will have a far-reaching impact on the sustainable development of human society. ^{3}He, an isotope of helium, is a clean, safe and controllable fusion fuel. Unfortunately, ^{3}He is rare on Earth (about 0.5 tons). It has been supposed that ^{3}He is very abundant in lunar rocks and soil grains [1, 2] due to the intense solar wind irradiation on the moon. Exploration of lunar resources, in particular ^{3}He, has become an inevitable trend in world space activities, because the resources not only provide energy for future lunar exploitation but also help to meet the growing energy needs on Earth [3, 4]. Determining the form of existence and the associated abundance of ^{3}He is crucial for effective usage of noble resources.

In previous works, the reservation of helium on the moon in different lunar rocks has been studied [5–8] either by *in situ* multispectral optical reflectance method [8] or *ex situ* analytical devices in laboratories [5, 6, 9]. It has been suggested that ilmenite is remarkably retentive of helium [5, 7, 8, 10–13]. Its helium content is closely correlated with the concentration of TiO_2 in ilmenite [6, 8]. The helium atoms were thought to be mostly retained in defects or as solid solutions in lunar regolith particles. Accordingly, the lattice of ilmenite particles is considered to be suitable for capturing ^{3}He [5, 10–12]. To extract the ^{3}He, high temperatures, e.g. 400 °C–1500 °C, are required [14, 15], because the diffusion rate that determines the release rate of ^{3}He is higher at high temperatures [16–18]. It was found that the concentration of helium is very rich in the region near the surface [19], and it is much higher than that predicted by simulations based on a diffusion model [20]. Therefore, it is intriguing to research why the surface layer can capture more helium.

In this work, we investigated the microstructures of lunar ilmenite particles brought back by Chang'E-5 [21–23] using an advanced spherical aberration-corrected transmission electron microscope (TEM) equipped with electron energy loss spectroscopy (EELS) and energy dispersive spectroscopy (EDS). It is found that there are huge amounts of helium bubbles in the glassy surface layer on the ilmenite particles. The glassy surface that is likely formed by irradiation acts as a reservoir to capture and retain helium gas owing to the superb stability of the lunar glass. We estimate the total reservation of helium gas on the moon according to our results.

1.1. Ilmenite particle identification

The Chang'E-5 samples studied in this work were scooped from the lunar regolith surface (samples CE5C0400), which comprise approximately 6.0% ilmenite, 44.5% pyroxene, 30.4% plagioclase, 15.5% glass phases, and 3.6% olivine [24]. To identify the ilmenite particles, the lunar regolith particles were loaded in a scanning electron microscope (SEM) and screened by using back-scattering mode, because the heavy elements, e.g. Fe and Ti are more sensitive in the back-scattering mode. Then, several ilmenite ($FeTiO_3$) particles containing Fe, Ti and O elements were identified and used for structural characterization. A representative ilmenite particle is shown in figure 1. Some agglutinates that mainly contain Ca, Al, Si, and O are attached to the ilmenite particle. A thin slice was cut from the ilmenite particle by using focused ion beam (FIB) for further TEM and EELS studies.

1.2. Helium bubbles

High-resolution transmission microscopy was applied to study the microstructure of ilmenite particles (see figure 2). As shown in figures 2(a)–(c), the top layer from the surface of the ilmenite particle is a glassy layer with dense disordered atomic packing structures (see the inset high-resolution TEM image). Its thickness is about 40–50 nm. Beneath the glassy layer is a partial glass region with a thickness of about 30 nm before reaching the inner crystalline phase. It is known that the irradiation of high-energy ions can induce the amorphization of crystalline materials, and the degree of the amorphization decreases with the increase of the depth [25–27]. Therefore, the top glass layer and the partially glassy layer beneath on the surface of the ilmenite should be attributed to the irradiation of the solar wind or other high-energy cosmic-ray irradiations.

Remarkably, we find plenty of spherical bubbles with diameters of about 5–25 nm in the glassy layer. Figure 2(d) shows the EELS curves acquired in different locations in figure 2(a). A strong helium peak at around 22 eV [10, 28] is detected in the big bubble (site 1 in figure 2(a)). The helium signal in the small bubble (site 2 in figure 2(a)) is weaker than that in the big bubble. The helium signal in the top glass layer (site 3 in figure 2(a)) is very weak and the signal in the crystalline phase (site 4 in figure 2(a)) is too weak to be detectable.

It can be seen that helium bubbles are mainly retained in the glassy layer (zoomed-in in figure 2(b)). It is noticeable that the helium bubbles are in spherical shapes with clear interfaces (figure 2(c)), which is attributed to the viscous and flowable characteristics of glasses [29–31]. These results suggest that the glassy layer plays a critical role in capturing and retaining helium gas.

The helium density is calculated following [32]: $n_{\mathrm{He}} = \frac{I_{\mathrm{He}}}{I_{\mathrm{ZIP}}\sigma_{\mathrm{He}}d}$, where n_{He} is the helium volume density (in He nm^{-3}); I_{He} is the integrated signal of helium; I_{ZIP} is the integrated intensity of the zero-loss peak; $\sigma_{\mathrm{He}} = 5.9 \times 10^{-6}$ N m^2 is the

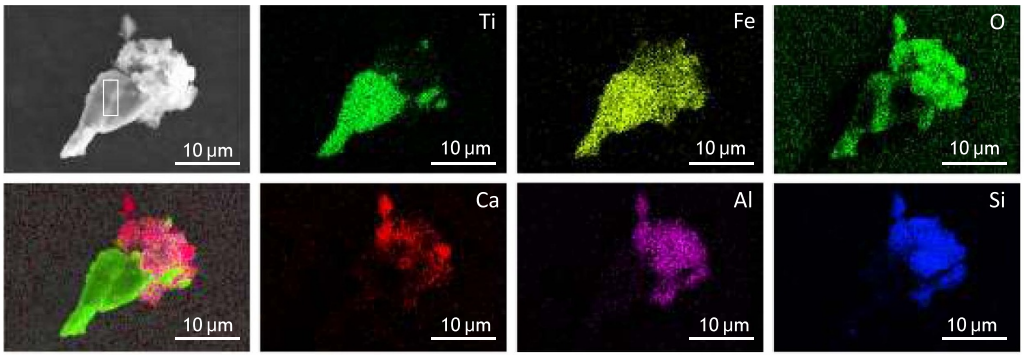

Figure 1. An SEM image and EDS elemental mapping for a representative ilmenite ($FeTiO_3$) particle with attachment of agglutinates. A thin layer is cut for TEM test from the white rectangle site in the first image.

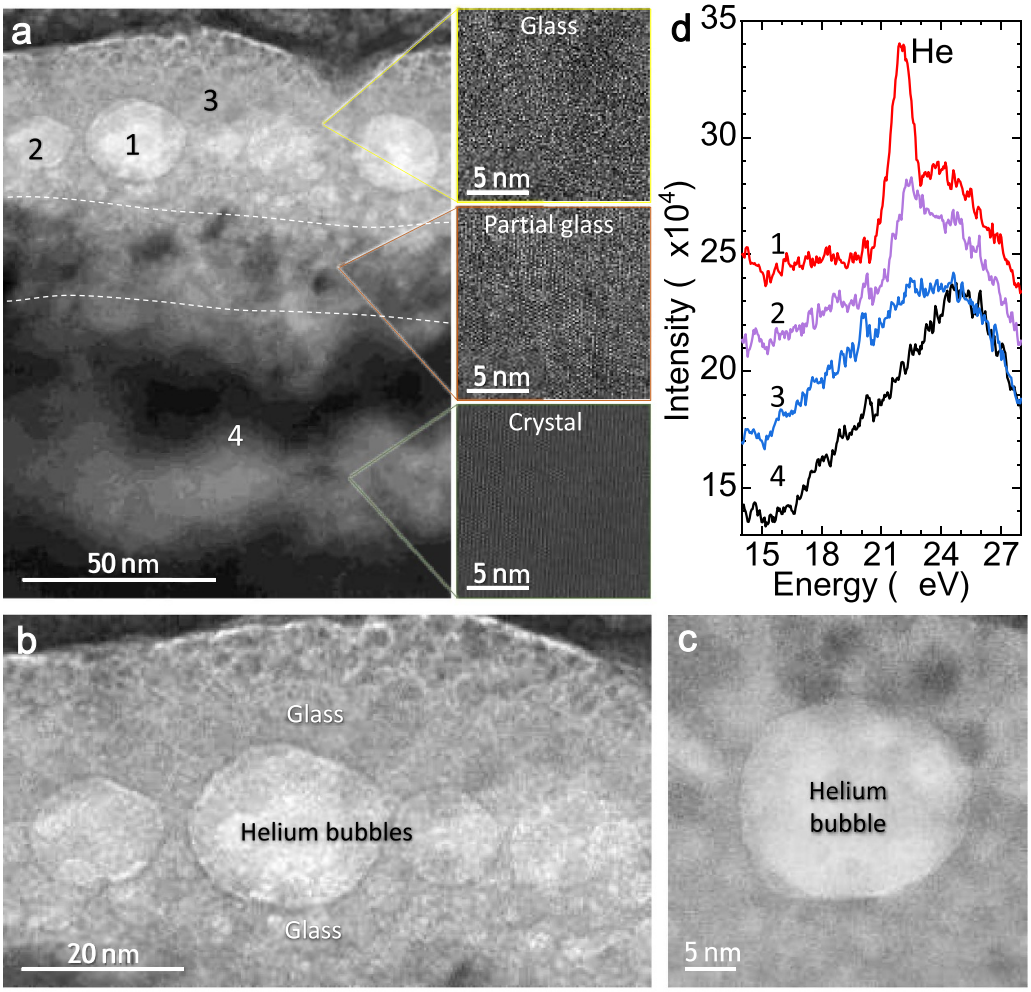

Figure 2. TEM images and EELS curves. (a) The bright field TEM image of the ilmenite ($FeTiO_3$) sample. It has a glassy surface layer of about 50 nm in thickness where abundant helium bubbles are observed. Below the glass layer is first a partial glass region and then the crystalline phase. On the right-hand side are high-resolution TEM images. (b) The zoomed-in image of the glass layer containing many helium gas bubbles. (c) A spherical helium bubble in the glass with clear interface. (d) The EELS curves acquired at different locations in (a); site 1 is a big bubble; site 2 is a small bubble; site 3 is in the glass layer; site 4 is in the crystalline phase. The helium signal at around 22 eV is detected in the glassy layer.

cross section for the He 1s-2p transition [28], and the d is the local thickness at the pixel position of the analyzed He nano-volume. The calculated helium volume density in different helium bubbles ranges from 50 to 192 He nm^{-3}. The pressure inside the bubbles is estimated according to [33, 34] to be about 1–39 GPa (see details in supplementary information, available online at stacks.iop.org/MF/1/035101/mmedia). The total mass of the helium gas in bubbles is estimated to be about

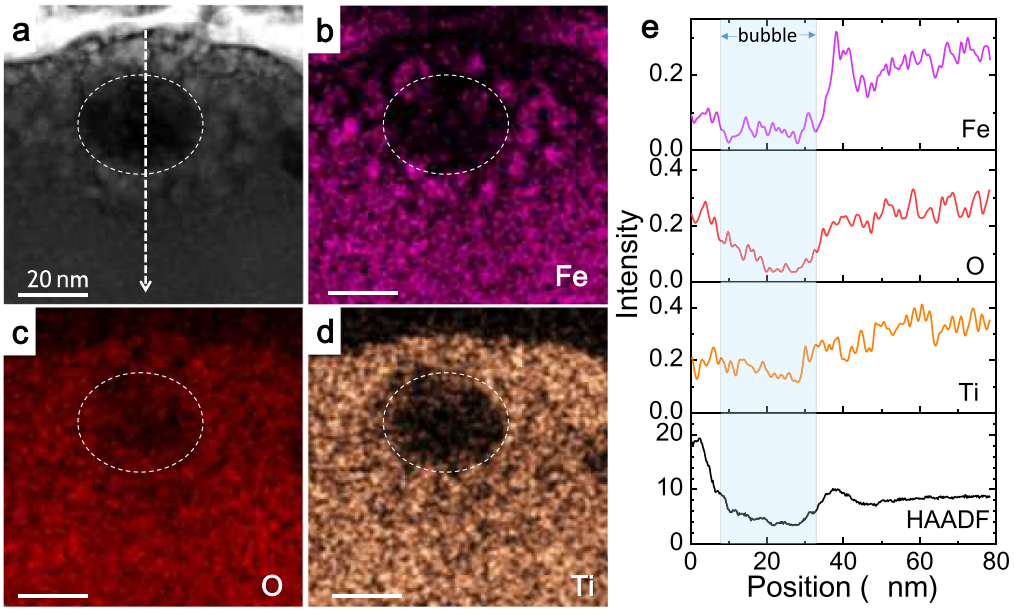

Figure 3. EDS mapping surrounding a helium bubble. (a) HAADF TEM image, and corresponding EDS mapping for (b) Fe, (c) O, and (d) Ti. The dashed circles are guiding eyes to the bubble outline. (e) The linear scan of elemental distribution across a helium bubble, see the dashed arrow in (a).

$M_{He} = (8.4–64.5) \times 10^{10}$ kg with a total volume of helium bubbles of about $(2.5–5) \times 10^8$ m^3 (details can be found in supplementary information). Upon the ratio of ^{3}He to ^{4}He is about 4×10^{-4} [35], the mass of ^{3}He in the bubbles should be up to 0.26×10^9 kg, which may be 1/10–1/4 of the total reserves of ^{3}He on the moon. According to the estimation by Wittenberg *et al* [3], the fusion energy produced by about 100 tons of ^{3}He could meet the global needs. Thus, the helium gas retained in lunar glass bubbles will be enough for the needs of about 2600 years on Earth.

Compared to the ^{3}He atoms captured in defects and in solid solutions that are difficult to extract, the helium gas in bubbles is of high quality, which is easier to extract. Mechanical methods at ambient temperatures, e.g. ball milling, can break the bubbles and efficiently release the gas. This is highly appreciated for *in situ* exploring the ^{3}He gas on the moon.

1.3. Formation and capture mechanisms of helium bubbles

It is intriguing to investigate how and why the helium bubbles were captured and retained in the glass layer. The elemental mapping of the region surrounding a helium bubble was studied by using EDS (figure 3). The Ti and O atoms distribute homogeneously across the glass layer while there are some Fe-rich nano-clusters surrounding the helium bubble. The precipitation of Fe clusters may be attributed to the reduction reaction by the hydrogen atoms in the solar wind. The glassy layer is mainly composed of TiO_2. Even though the solar wind irradiation spans billions of years [24], the damage is limited to a thin layer of only 50 nm. This denotes a high irradiation tolerance of ilmenite, especially with the protection of a glassy layer whose disordered atomic packing structure can greatly decrease the speed of ions in the solar wind.

A schematic illustration for the process to capture and retain the helium gas in ilmenite is shown in figure 4. The ilmenite lattice is more suitable for helium atoms to implant compared to other lunar regolith particles [36, 37]. The high-speed ions in the solar wind implant into the lattice and are trapped in the vacancies and interstitials (figure 4(a)). After a long-time irradiation, the lattice close to the surface is damaged and forms a glassy layer (figures 2 and 4(b)). Even though the crystalline ilmenite can capture many helium atoms, it could not retain them because of the channeling effect of crystalline lattice [38], that is, some orientation in a lattice structure is easier for ions to implant and release. In addition, the hot-cool cycles on the moon promote the release of these trapped atoms in the lattice. When the helium atoms diffuse into the surface glassy TiO_2 layer with disordered and densely packed structure, there is no crystalline tunneling effect, and helium atoms are difficult to escape from the disordered structure and are then retained and form bubbles in the glass. This is the reason why the EELS results show that the helium concentration in the inner crystalline structure is much lower than that in the glassy surface, especially that the helium bubbles all locates in the glassy layer. The ultrahigh stability [39, 40] and dense atomic packing structure [41] of TiO_2 glass can retain the helium gas for ultra-long time. The high pressure in the helium bubbles of about 1–39 GPa also confirms that the glassy TiO_2 is an ideal reservoir to retain helium gas.

In summary, even though the lunar regolith brought back by Chang'E-5 mission is much younger than those from the Apollo mission and Luna mission, it contains large amounts of ^{3}He resource. The ^{3}He gas that is stored in bubbles in

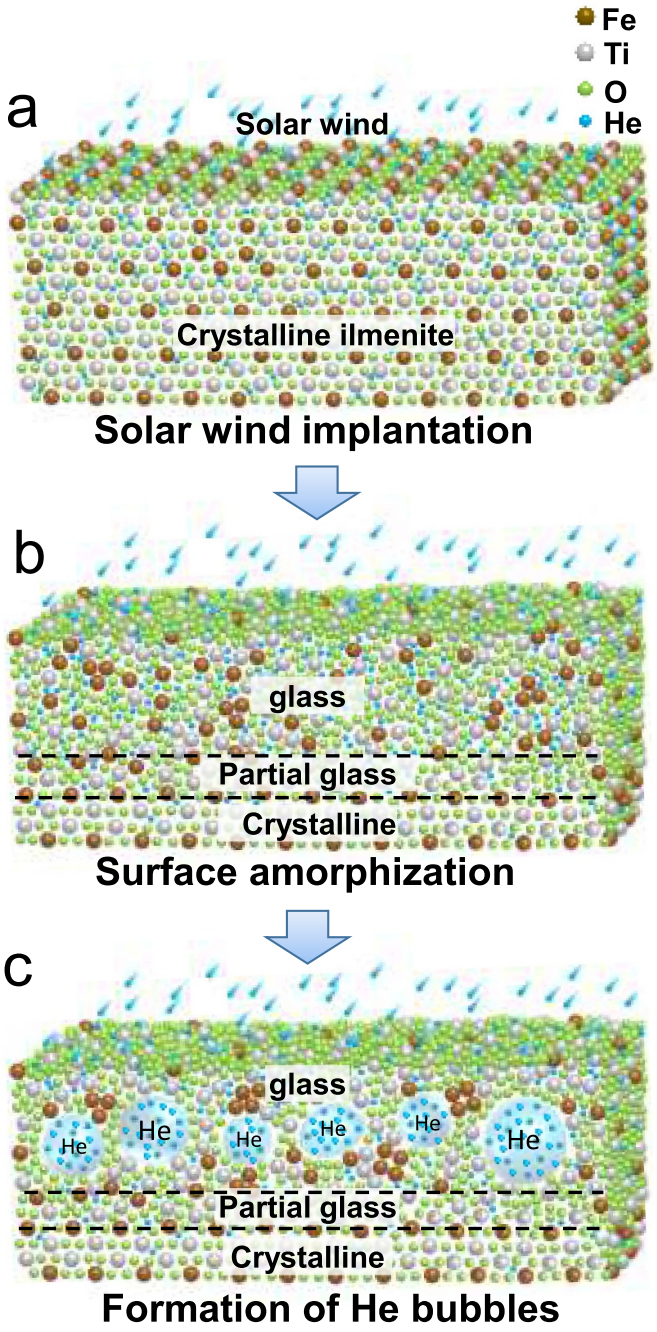

Figure 4. Schematic illustration of the capturing and retaining process of helium (He) on the surface of ilmenite. (a) Helium atoms in the solar wind implant into the lattice of crystalline ilmenite. (b) Surface amorphization caused by long-time irradiation of the solar wind. (c) Helium atoms diffuse into the glassy surface layer and form bubbles.

the glassy surface layer of the ilmenite particles is more convenient to extract *in situ* compared to the ^{3}He atoms retained in lattice defects. This work provides a first evidence for the advantage of glass in capturing and retaining ^{3}He on the moon owing to its stable disordered atomic packing structure, which acts as a reservoir of the noble ^{3}He gas. Our findings suggest the possibility for future exploration of ^{3}He resource on the moon.

2. Methods

2.1. Sample preparation

The Chang'E-5 samples studied in this research were scooped from the lunar regolith surface (samples CE5C0400), which comprises approximately 44.5% pyroxene, 30.4% plagioclase, 15% glass phase, 6.0% ilmenite, and 3.6% olivine. A small number of samples were examined under a binocular optical microscope, Ningbo Yongxin NM910, in an ultraclean environment provided by a glovebox (Mikrouna Inc.). The particles with a size ranging from a few microns to dozens of microns were hand-picked and then transferred to a sticky carbon substrate. The selected particles were characterized by morphologic observations and the elemental mapping in a field emission SEM, Thermo Scientific Verios G4 UC, with the following parameter: acceleration voltage of 15.0 kV and probe current of 3.2 nA. Under the back-scattering mode, the particles containing heavy elements were confirmed and then EDS mappings were acquired on each particle to screen out particles rich in Fe and Ti elements. The FeTi-rich particles were selected to prepare the sections using FIB microscopy with a FEI Helios G4 CX. Regions of interest on the chosen particles were coated with a thick ion beam deposited Pt film ($\sim$1 μm) before ion milling to prevent damage to the particle surface by the ion beam.

2.2. Scanning transmission electron microscope (STEM)-EELS measurements

STEM imaging was performed on a spherical aberration-corrected STEM instrument, Thermo Fisher Spectra 300, equipped with a 5th order aberration corrector. The instrument provided an incident electron probe of $\sim$1.3 Å in full-width-at-half-maximum with a convergent semiangle of 24.6 rad. The beam current of the electron probe is set to be $\sim$50 pA and a typical dose level of $\sim$0.4–1 $\times$ 10^{8} N m^{2} as used for high-resolution imaging. STEM measurements were conducted at 300 kV accelerating voltage under an ultra-high vacuum level of $\sim$1 $\times$ 10^{-7} Pa. STEM images were acquired in bright field mode and high-angle annular dark field (HAADF) mode, respectively. As will be discussed later, a layer containing many bubbles, which is located at $\sim$10 nm below the sample surface, was observed via STEM. In order to detect the helium, EELS acquisitions were conducted and recorded through a Gatan 1066 with a collection semiangle of 50 rad. The energy resolution determined by the full width at half maximum of the zero-loss peak was approximately 0.5 eV. The EELS mappings were carried out on the regions containing the bubbles. We carefully acquired the EELS signal from the central portion of each bubble for the following accurate estimation of helium density in the bubbles. EDS maps of the He bubbles regions were collected with a Thermo Fisher EDS detector with four probes. Data for EELS and EDS were acquired as spectrum images. The EELS and EDS data analysis were performed using the Digital Micrograph software (Gatan Inc.) and Velox software (Thermo Fisher Inc.), respectively.

Data availability statement

The data that support the findings of this study are available within the article and the Supplementary Information.

Acknowledgments

We thank all the staff of China's Chang'E Lunar Exploration Project for their hard work in returning lunar samples and China National Space Administration (CNSA) for providing the lunar sample. The support from Qian Xuesen Laboratory of Space Technology and the financial support from National Natural Science Foundation of China (NSFC 51922102, 92163108, 61888102, 11790291), and Youth Innovation Promotion Association CAS (2019296), Zhejiang Provincial Natural Science Foundation of China (LZ22A030001, LR22E010004), Ningbo 2025 Science and Technology Innovation Project (2022Z033) are acknowledged.

Author contributions

W H W, H Y B, M F Y, Z G Z and S F Z led and supervised this project. J Q W, W X and J T H conceived and guided the research. A L, X C, L J S, M G, M J, Y Z prepared the samples. G C, M L, L Z, A L, X C conducted the TEM and EELS measurements. J Q W, W X, J T H, L J S, Y H L, H Y B, W H W wrote the manuscript. All authors discussed the results and contributed to the preparation of the manuscript.

Conflict of interest

The authors declare no competing interests.

ORCID iDs

Yan Zhang https://orcid.org/0000-0002-1178-8177
Jun-Qiang Wang https://orcid.org/0000-0002-8066-6237

References

[1] Eberhardt P, Geiss J, Graf H, Grögler N, Krähenbühl U, Schwaller H, Schwarzmüller J and Stettler A 1970 Trapped solar wind noble gases, Kr^{81}/Kr exposure ages and K/Ar ages in Apollo 11 lunar material *Science* **167** 558–60
[2] Jordan J L 1990 Mapping pyroclastic deposits and other lunar features for solar wind implanted helium, lunar volcanic glasses: scientific and resource potential *LPI Tech. Rep.* (Texas) pp 43–45
[3] Wittenberg L J, Santarius J F and Kulcinski G L 1986 Lunar source of ^{3}He for commercial fusion power *Fusion Technol.* **10** 167–78
[4] Kulcinski G L and Schmitt H H 1988 The moon: an abundant source of clean and safe fusion fuel for the 21st century *Lunar Helium-3 and Fusion Power NASA Conf. Publication 10018* (*Washington*) pp 35–63
[5] Harris-Kuhlman K R 1998 Trapping and diffusion of helium in lunar minerals (The University of Wisconsin-Madison)
[6] Johnson J R, Swindle T D and Lucey P G 1999 Estimated solar wind-implanted helium-3 distribution on the Moon *Geophys. Res. Lett.* **26** 385–8
[7] Taylor L A 1994 *Helium-3 on the Moon: Model Assumptions and Abundances, Engineering, Construction, and Operations in Space IV* (New York: American Society of Civil Engineers) pp 678–86
[8] Fa W and Jin Y-Q 2007 Quantitative estimation of helium-3 spatial distribution in the lunar regolith layer *Icarus* **190** 15–23
[9] Keller L P and Mckay D S 1993 Discovery of vapor deposits in the lunar regolith *Science* **261** 1305–7
[10] Burgess K D and Stroud R M 2018 Phase-dependent space weathering effects and spectroscopic identification of retained helium in a lunar soil grain *Geochim. Cosmochim. Acta* **224** 64–79
[11] Signer P, Baur H, Derksen U, Etique P, Funk H, Horn P and Wieler R 1977 Helium, neon, and argon records of lunar soil evolution *Proc. 7th Lunar Science Conf.* (New York: Pergamon Press) pp 3657–83
[12] Christoffersen R, Keller L P and Mckay D S 1996 Microstructure, chemistry, and origin of grain rims on ilmenite from the lunar soil finest fraction *Meteorit. Planet. Sci.* **31** 835–48
[13] Keller L P and McKay D S 1997 The nature and origin of rims on lunar soil grains *Geochim. Cosmochim. Acta* **61** 2331–41
[14] Futagami T, Ozima M, Nagal S and Aoki Y 1993 Experiments on thermal release of implanted noble gases from minerals and their implications for noble gases in lunar soil grains *Geochem. Cosmochim. Acta* **57** 3177–94
[15] Srinivasan B, Hennecke E W, Sinclair D E and Manuel O K 1972 A comparison of noble gases released from lunar fines (15601.64) with noble gases in meteorites and in the earth *Proc. 3rd Lunar Science Conf.* (MIT Press) pp 1927–45
[16] Heiken G, Vaniman D and French B 1991 *Lunar Sourcebook* (New York: Cambridge University Press)
[17] Zhang L, Wu K, Chen Z, Yu X, Li J, Yang S, Hui G and Yang M 2021 Gas storage and transport in porous media: from shale gas to helium-3 *Planet. Space Sci.* **204** 105283
[18] Ducati H, Kalbitzer S, Kiko J, Kirsten T and Müller H W 1973 Rare gas diffusion studies in individual lunar soil particles and in artificially implanted glasses *Moon* **8** 210–27
[19] Mueller H W, Jordan J, Kalbitzer S, Kiko J and Kirsten T 1976 Rare gas ion probe analysis of helium profiles in individual lunar soil particles *Proc. Lunar Science Conf. 7th* vol 1 pp 937–51
[20] Kiko J, Kirsten T and Ries D 1978 Distribution properties of implanted rare gases in individual olivine crystals from the lunar regolith *Proc. Lunar Planet. Science Conf. 9th* vol 9 pp 1655–65
[21] Hu S *et al* 2021 A dry lunar mantle reservoir for young mare basalts of Chang'e-5 *Nature* **600** 49–53
[22] Tian H C *et al* 2021 Non-KREEP origin for Chang'e-5 basalts in the Procellarum KREEP Terrane *Nature* **600** 59–63
[23] Li Q L *et al* 2021 Two-billion-year-old volcanism on the Moon from Chang'e-5 basalts *Nature* **600** 54–58
[24] Zhang H *et al* 2021 Size, morphology, and composition of lunar samples returned by Chang'E-5 mission *Sci. China-Phys. Mech. Astron.* **65** 229511
[25] Weber W J 2000 Models and mechanisms of irradiation-induced amorphization in ceramics *Nucl. Instrum. Methods Phys. Res.* B **166–167** 98–106
[26] Snead L L, Zinkle S J, Hay J C and Osborne M C 1998 Amorphization of SiC under ion and neutron irradiation *Nucl. Instrum. Methods Phys. Res.* B **141** 123–32
[27] Okubo N, Ishikawa N, Sataka M and Jitsukawa S 2013 Surface amorphization in Al_2O_3 induced by swift heavy ion irradiation *Nucl. Instrum. Methods Phys. Res.* B **314** 208–10

[28] Evin B, Leroy E, Segard M, Paul-Boncour V, Challet S, Fabre A and Latroche M 2021 Investigation by STEM-EELS of helium density in nanobubbles formed in aged palladium tritides *J. Alloys Compd.* **878** 160267
[29] Cao C R, Lu Y M, Bai H Y and Wang W H 2015 High surface mobility and fast surface enhanced crystallization of metallic glass *Appl. Phys. Lett.* **107** 141606
[30] Zhu L, Brian C W, Swallen S F, Straus P T, Ediger M D and Yu L 2011 Surface self-diffusion of an organic glass *Phys. Rev. Lett.* **106** 256103
[31] Malshe R, Ediger M D, Yu L and de Pablo J J 2011 Evolution of glassy gratings with variable aspect ratios under surface diffusion *J. Chem. Phys.* **134** 194704
[32] Walsh C A, Yuan J and Brown L M 2000 A procedure for measuring the helium density and pressure in nanometre-sized bubbles in irradiated materials using electron-energy-loss spectroscopy *Phil. Mag.* A **80** 1507–43
[33] Trinkaus H 2006 Energetics and formation kinetics of helium bubbles in metals *Radiat. Eff.* **78** 189–211
[34] David M L, Alix K, Pailloux F, Mauchamp V, Couillard M, Botton G A and Pizzagalli L 2014 *In situ* controlled modification of the helium density in single helium-filled nanobubbles *J. Appl. Phys.* **115** 123508
[35] Ivanov A V 2014 Volatiles in lunar regolith samples: a survey *Sol. Syst. Res.* **48** 113–29
[36] Song H, Zhang J, Sun Y, Li Y, Zhang X, Ma D and Kou J 2021 Theoretical study on thermal release of helium-3 in lunar ilmenite *Minerals* **11** 319
[37] Mueller H, Jordan J, Kalbitzer S, Kiko J and Kirsten T 1976 Rare gas ion probe analysis of helium profiles in individual lunar soil particles *Proc. 7th Lunar Science Conf.* (New York: Pergamon Press) pp 937–51
[38] Cho K, Allen W R, Finstad T G, Chu W K, Liu J and Wortman J J 1985 Channeling effect for low energy ion implantation in Si *Nucl. Instrum. Methods Phys. Res.* B **7–8** 265–72
[39] Nie X, Wang J, Duan W, Zhao Z, Li L and Zhang Z 2021 Effects of different crystallization methods on photocatalytic performance of TiO_2 nanotubes *Appl. Phys.* A **127** 879
[40] Fromknecht R, Auer R, Khubeis I and Meyer O 1996 Lattice location and electrical conductivity in ion implanted TiO_2 single crystals *Nucl. Instrum. Methods Phys. Res.* B **120** 252–6
[41] Zhang H, Chen B, Banfield J F and Waychunas G A 2008 Atomic structure of nanometer-sized amorphous TiO_2 *Phys. Rev.* B **78** 214106